

Numerical simulation of bridge piers with spread footings under earthquake excitation

Jiunn-Shyang Chiou^{*1}, Yi-Wun Jheng^{1a} and Hsiao-Hui Hung^{2b}

¹Department of Civil Engineering, National Taiwan University,
No. 1, Section 4, Roosevelt Rd., Taipei, Taiwan 10617, Republic of China

²National Center for Research on Earthquake Engineering, 200, Section 3, Xinhai Rd., Taipei, Taiwan 10668, Republic of China

(Received February 11, 2019, Revised April 2, 2019, Accepted April 4, 2019)

Abstract. This study simulates the responses of large-scale bridge piers under pseudo-dynamic tests to investigate the performance of four types of numerical models that consider the nonlinear behavior of the pier and the rocking behavior of the footing. In the models, beam-column elements with plastic hinges are used for the pier, two types of foundation models (rotational spring and distributed spring models) are adopted for the footing behavior, and two types of viscous damping models (Rayleigh and dashpot models) are applied for energy dissipation. Results show that the nonlinear pier model combined with the distributed spring-dashpot foundation model can reasonably capture the behavior of the piers in the tests. Although the commonly used rotational spring foundation model adopts a nonlinear moment-rotation property that reflects the effect of footing uplift, it cannot suitably simulate the hysteretic moment-rotation response of the footing in the dynamic analysis once the footing uplifts. In addition, the piers are susceptible to cracking damage under strong seismic loading and the induced plastic response can provide contribution to earthquake energy dissipation.

Keywords: damping; plastic hinges; rocking; seismic design; spread footings; Winker models

1. Introduction

A spread footing is a typical type of foundation for bridge structures located on firm ground (rock or gravel strata). When a bridge pier with spread footings is subjected to strong seismic loading, the pier may have a plastic response due to plastic hinging. On the other hand, the foundation is likely to rock because of shallow embedment. Therefore, the overall seismic response of bridge piers with spread footings under seismic loading is influenced by both the pier and foundation behaviors.

Following the capacity design method, the seismic design method of bridge structures generally involves allowing plastic hinging occurring in piers to develop ductile failure during strong earthquakes. In this way, other undesirable failure types occurring at other locations, such as the foundations, can be avoided. Therefore, many studies focusing on a pier's energy dissipation capability have been conducted to examine the ductile behavior of piers (Billington and Yoon 2004, Galal 2007, Chen *et al.* 2011, Wang *et al.* 2014).

On the other hand, foundation rocking may cause a reduction in the acceleration response of a structure and

lead to another form of seismic isolation (Mergos and Kawashima 2005, Sakellarakis and Kawashima 2006, Apostolou *et al.* 2007, Gajan and Kutter 2008). Thus, recently, this mechanism was suggested as an alternative to the aforementioned conventional seismic design method. However, when performing rocking foundation design, it is necessary to check the stability of the pier subjected to a large lateral displacement at the top of the pier due to foundation rocking (Standards New Zealand 2004, AASHTO 2009, Ni 2013, Deng *et al.* 2014). Many experimental studies using shaking table tests and centrifuge tests have been performed to study the mechanism and performance of rocking foundations (Gajan and Kutter 2008, Shirato *et al.* 2008, Hung *et al.* 2011, 2014, Antonellis *et al.* 2015, Chiou *et al.* 2018). Gajan and Kutter (2008) conducted several series of centrifuge model tests to investigate the rocking effect of shear wall foundations under seismic loading. They built relationships for the moment capacity, energy dissipation, and permanent settlement of foundations with a critical contact area between the soil and foundation. Hung *et al.* (2011) performed a series of cyclic load tests and pseudo-dynamic tests on large-scale bridge piers; their experimental results confirmed that foundation rocking behavior was beneficial to seismic isolation, but it resulted in an increased lateral displacement at the top of the piers. Antonellis *et al.* (2015) conducted a series of shaking table tests of large-scale bridge piers with rocking shallow foundations using a large outdoor shaking table and a large soil confinement box. They found that the properties of the soil around foundations significantly affected the residual displacement, residual rotation and re-centering capability of the

*Corresponding author, Assistant Professor

E-mail: jschiou@ntu.edu.tw

^aFormer Master Student

E-mail: yiwun0430@gmail.com

^bResearch Fellow

E-mail: hhung@narlabs.org.tw

foundations.

Many analysis methods have been developed to model foundation rocking behavior. The rotational spring model is a commonly used model (Deng *et al.* 2014, Lu *et al.* 2016) that connects an equivalent rotational spring to the bottom of the column to represent foundation flexibility. The moment-rotation property of the rotational spring can be expressed as a nonlinear curve in order to consider the effects of soil nonlinearity and uplift of the footing (Allotey and El Naggar 2003, Deng *et al.* 2014, Chiou *et al.* 2018). A macro spring model was further developed considering the coupled effects of shear, bending, and axial loadings on the capacity of footings (Grange *et al.* 2008, Paolucci *et al.* 2008, Anastasopoulos and Kontoroupi 2014). On the other hand, to simulate a more detailed foundation-soil interaction behavior, a distributed spring model that applies compression-only springs beneath the bottom of the footing was proposed (ASCE 2000, Allotey and El Naggar 2007, Raychowdhury and Hutchinson 2009, Deng *et al.* 2012). Compared to the rotational spring model, the distributed spring model can easily and directly consider the energy dissipation behavior of the footing.

Most experimental studies have explored the effects of the nonlinear behavior of pier and foundation rocking separately, while tests that consider the combined effects are limited. Hung *et al.* (2011, 2014) carried out several series of pseudo-dynamic tests on pier specimens with spread footings to investigate the interactive effects of pier nonlinearity and foundation rocking on pier responses. Focusing on the footing rocking behavior, they used a neoprene pad to simulate a footing on stiff ground, ignoring the influence of soil nonlinearity. They found that both the pier and foundation behaviors affected the total behavior of the pier, and that the ratio of the moment capacities of the footing and the pier determines whether the final response of the pier is governed by the pier or footing or both. Therefore, it is essential to simulate the behaviors of the foundation and the pier for the actual response of a bridge structure under seismic loading (Deng *et al.* 2012, Chaudhary 2017). In the current practice of nonlinear structural analysis, the nonlinear behavior of a pier is usually modeled using nonlinear beam-column elements or the plastic hinge model. For the foundation behavior, despite the development of complex numerical modeling schemes, the spring model is still popular because of its simplicity, especially the rotational spring model. However, the performance of a combined model considering both pier nonlinearity and the effect of foundation rocking on the pier response has not been explored extensively. Besides, since the rocking behavior of a foundation is usually accompanied by soil yielding, the simulation details in dynamical analysis for the energy-dissipation mechanism purely due to foundation uplift, and their influences on the analysis results have not been clearly investigated.

Therefore, by simulating the pseudo-dynamic tests on pier specimens with spread footings conducted by Hung *et al.* (2014), this study investigates the performance of four types of numerical models that consider the nonlinear behavior of the pier and the rocking behavior of the footing. The models are established using beam-column elements to

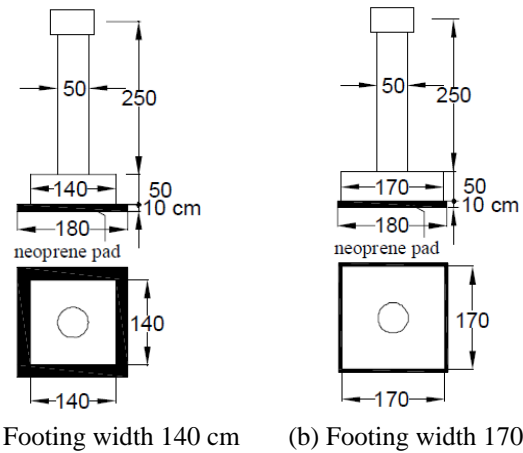


Fig. 1 Dimensions of test pier specimens: (a) CD40FS-R, (b) CD40FB-R (Hung *et al.* 2014)

simulate the pier specimens and applying spring models to simulate the footing behavior. The distributed plastic hinge model is applied for the nonlinear flexural behavior of the pier, and the Takeda restoring force model is used for the post-yield hysteretic response. Since, in the tests, a neoprene pad was placed beneath the footing to represent a spread footing on stiff soil, two types of foundation models, the rotational spring model and the distributed spring model, are adopted, assuming an elastic subgrade. Furthermore, since damping is another key factor that influences the dynamic responses of a structure, modeling of the damping is also evaluated in this study. The influences of two types of viscous damping models are compared: the Rayleigh and dashpot damping models. According to this comparison, the ability of the foundation spring models to capture the energy-dissipation mechanism of the foundation uplift is investigated. Finally, an appropriate model for the seismic responses of piers with spread footings on firm ground is recommended.

2. Overview of Hung *et al.*'s experiments

Hung *et al.* (2014) performed a series of large-scale lateral loading tests on bridge pier specimens. Six specimens including three piers with different reinforcement ratios and two footing sizes were made. The present study focuses on two of the specimens: CD40FS-R (small-size footing) and CD40FB-R (large-size footing).

Specimens CD40FS-R and CD40FB-R had the same reinforcement ratio but different footing sizes: 140 cm×140 cm and 170 cm×170 cm, respectively, as shown in Fig. 1. The height of the piers was 2.5 m. The structural details of the pier cross section included eighteen D19 longitudinal bars (reinforcement ratio 2.63%) and a D13 perimeter hoop (spacing 9 cm, reinforcement ratio 1.2%). The yield strength of longitudinal and transverse steels was $f_y=412$ MPa and the compressive strength of concrete was $f'_c=27.5$ MPa. The spread footings were situated on a 10-cm-thick, 180-cm×180-cm neoprene pad (Duro-60, the modulus of elasticity and the shear modulus are 4.45 and 1.06 MPa,

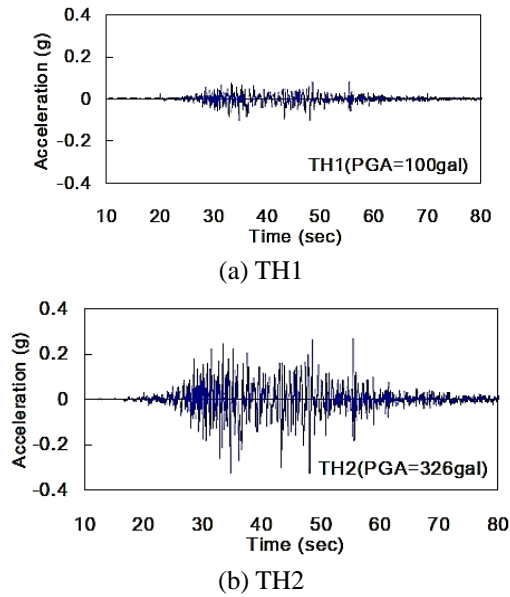
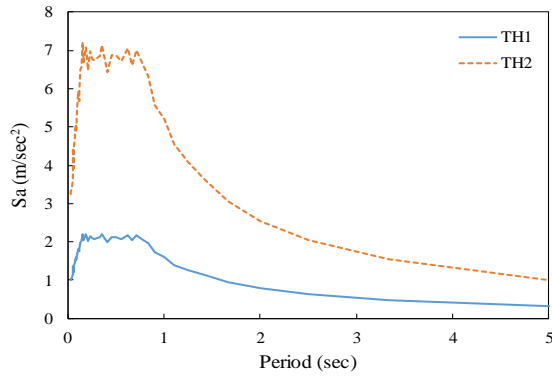

 Fig. 2 Input motions (Hung *et al.* 2014)


Fig. 3 Acceleration spectra of input motions

respectively) to simulate a footing on stiff ground, having an equivalent coefficient of subgrade reaction of around 480-520 MN/m³ (Terzaghi 1955). In the tests, an axial load of 539 kN was applied on the top of the piers to simulate the weight of a superstructure.

The test sequence included a pseudo-dynamic test followed by a cyclic loading test. The input ground motions TH1 and TH2 for the pseudo-dynamic tests and the associated acceleration spectra are shown in Figs. 2 and 3, respectively. They were artificial spectrum-compatible earthquake acceleration histories for Pouli, Nantou, a region of high seismicity in Taiwan. TH1 and TH2 had intensities with peak ground accelerations (PGA) of 100 and 326 gal, respectively. In the pseudo-dynamic test, an actuator attached on the top of the pier was given commands step by step to achieve the set target displacements for the entire excitation history. The target displacement for each time step was calculated by means of the equation of motion of a single-degree-of-freedom system based on the reaction force measured from the former time step and the prescribed values of mass and damping. After the pseudo-dynamic test, a cyclic test was further performed under displacement control to a drift ratio of 7% (17.5 cm).

3. Numerical models

In this study, four types of numerical models are adopted to simulate the pseudo-dynamic tests of the pier specimens (CD40FS-R and CD40FB-R). The models are established in the SAP2000 platform (Computers and Structures 2017), as shown in Fig. 4. The models have four parts: a lumped mass for the superstructure (pseudo-dynamic test condition), beam-column elements for the pier, a rigid link for the footing slab, and spring models for the reactions from the pad. The main differences between these four models are the foundation models for the reactions from the pad (rotational spring model and distributed spring model) and the viscous damping models for energy dissipation (Rayleigh and dashpot damping models). Details of the pier models, the foundation models, and the associated damping models adopted for each of the four models are described below.

3.1 Pier models

The pier models in Models I-IV are the same except for the viscous damping. Linearly elastic beam-column elements are used to simulate the pier. To consider the plastic behavior of the pier, the distributed plastic hinge model (Chiou *et al.* 2009) is applied by placing plastic hinges along the beam-column elements. The properties of the plastic hinges are set based on the moment-curvature curve of the pier cross-section. According to this curve, the moment-rotation curve of the plastic hinges is determined by multiplying the plastic curvature by the tributary length of the hinges, in which the plastic curvature ϕ_p is defined as (Chiou *et al.* 2009)

$$\phi_p = \phi - \frac{M}{EI_e} \quad (1)$$

where EI_e is the effective flexural rigidity, M is the bending moment, and ϕ is the total curvature for the bending moment M .

When the pier enters the inelastic state, the hysteretic restoring force model is set along with the plastic hinge model to simulate the loading-unloading behavior. SAP 2000 provides some hysteretic restoring force models, including isotropic, kinematic, Takeda, pivot, etc. In this study, the Takeda model (Takeda *et al.* 1970), which is commonly used in structural dynamic analysis for reinforced concrete members, is adopted.

Before the pier yields, the above hysteretic damping model does not actually work and therefore the viscous damping model is applied to consider the energy dissipation in the elastic stage. In this study, the Rayleigh damping model (for Models I and III) and the dashpot damping model (for Models II and IV) are adopted to account for the viscous damping. The details of the viscous damping models are described later, including those adopted in the foundation models.

3.2 Foundation models

Two types of foundation models are used: the equivalent

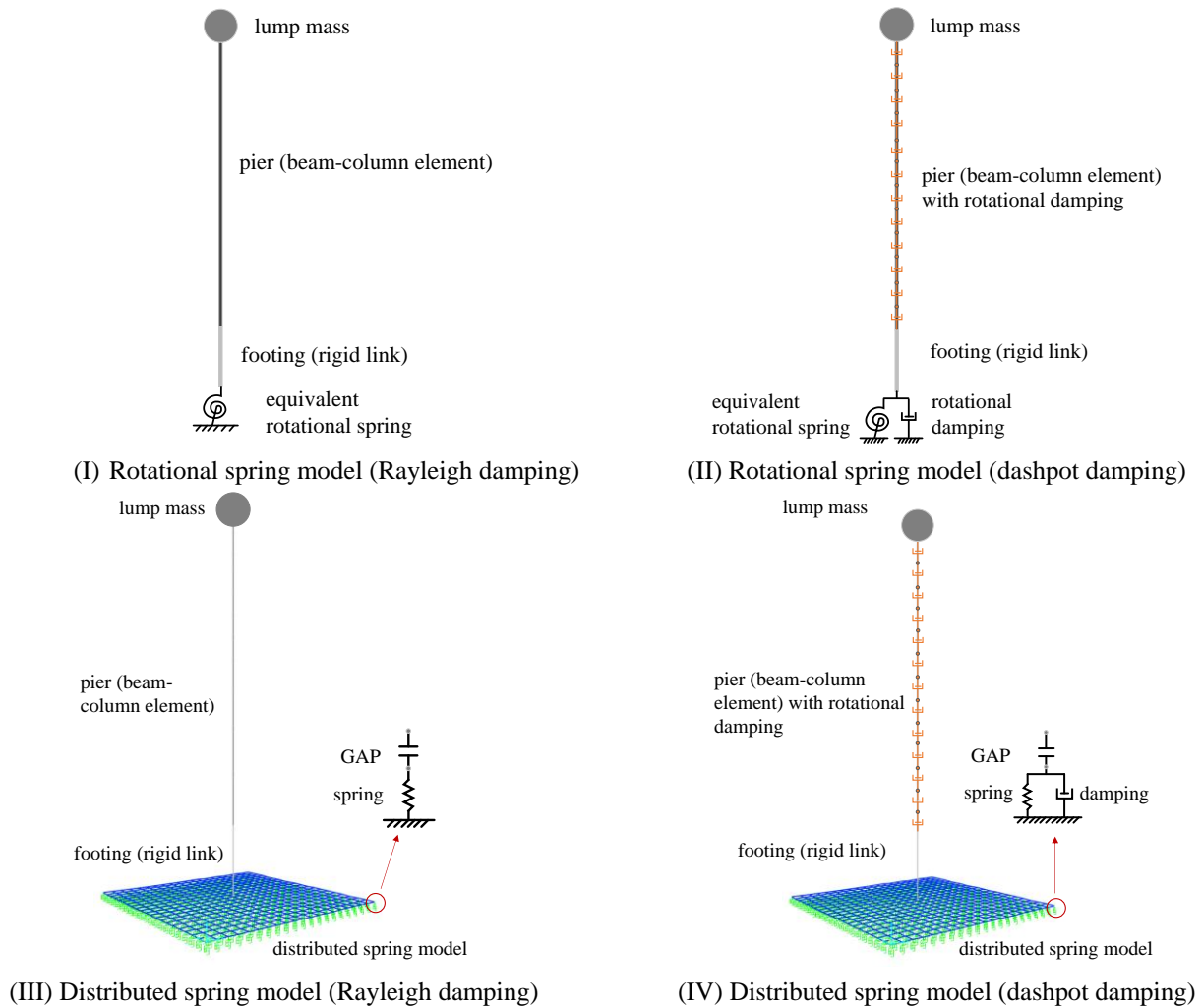


Fig. 4 Numerical models

rotational spring model (Models I and II) and the distributed spring model (Model III and IV). In the rotational spring model, an equivalent rotational spring for the rocking behavior of a footing is built based on the analytical moment-rotation relationship of the footing. For a footing with width B and length L situated on an elastic subgrade with a coefficient of vertical subgrade reaction k_v , the analytical moment-rotation relationship of the footing for a moment that acts in the longitudinal direction of the footing can be expressed as follows (JRA 2012, Chiou *et al.* 2018):

Before the footing uplifts ($\theta \leq \theta_0$), the moment-rotation relationship of the footing is linear

$$M = M_0 \frac{\theta}{\theta_0} \quad \text{and} \quad (2-1)$$

After the footing uplifts ($\theta > \theta_0$), the contact area between the footing base and the soil decreases and therefore the moment-rotation relationship of the footing becomes nonlinear

$$M = M_0 \left(3 - 2\sqrt{\frac{\theta_0}{\theta}} \right) \quad (2-2)$$

where M_0 and θ_0 are the moment and the corresponding

rotation, respectively, at which the footing begins to uplift ($M_0 = BP/6$, $\theta_0 = \frac{2P}{k_v LB^2}$, where P is the axial load). The

square root of θ_0/θ represents the ratio of the contact area to the total area of the footing base (contact area ratio). When the footing rotation θ is much larger than θ_0 , the contact area ratio will be close to zero and the moment will approach the ultimate moment of $3M_0$.

For the distributed spring model, the Winkler foundation model is applied to simulate the footing base reactions using a bed of independent vertical springs. Each spring is composed of a gap element connected in series with a general two-way spring element (for both compression and tension sides). The force-displacement relationship of the gap element, which only has compressive stiffness, is shown in Fig. 5. The function of the gap element is to transmit the compressive force to the two-way spring, but not to contribute to the displacement. Therefore, the gap element is assigned a very large stiffness in order to only produce very small displacements when loaded.

In these two types of foundation models, the key parameter is the coefficient of vertical subgrade reaction, k_v . This study performs finite-element analyses to determine k_v

values for the neoprene pad. For example, for the small-size footing (CD40FS-R), a three-dimensional model in ABAQUS (Hibbit *et al.* 2000) is constructed for the foundation slab, pad and floor, as shown in Fig. 6. The vertical displacement is analyzed by applying pressure on the top of the foundation slab. The ratio of the vertical displacement of the pad to the applied pressure gives the value of k_v . In this way, the deduced k_v values for CD40FS-R and CD40FB-R are 485 and 516 MN/m³, respectively.

Regarding the neoprene pad as an elastic material, the nonlinearly elastic rotational spring or linearly elastic distributed springs in the foundation models are set without plastic responses. Therefore, viscous damping is introduced to consider the energy dissipation in the elastic response.

3.3 Viscous damping models

Rayleigh damping model (damping for the whole system)

In structural dynamic analysis, Rayleigh damping is commonly used to simulate energy dissipation in an elastic system. Rayleigh damping uses two coefficients, α and β , to proportionally combine the mass and stiffness matrices to form a damping matrix. The following simultaneous equations are built to determine the coefficients α and β :

$$\begin{aligned} \alpha + \beta\omega_1^2 &= 2\xi_1\omega_1 \\ \alpha + \beta\omega_2^2 &= 2\xi_2\omega_2 \end{aligned} \quad (3)$$

where ω_1 and ω_2 are two specific system frequencies and ξ_1 and ξ_2 are the damping ratios corresponding to ω_1 and ω_2 .

Based on previous studies (e.g., Gajan and Kutter 2008) and Hung *et al.*'s test results (Hung *et al.* 2014), the equivalent damping ratio for a rocking system seemed insensitive to the rotation level of the footing. Therefore, assume $\xi_1 = \xi_2 = \xi$:

$$\alpha = \xi \frac{2\omega_1\omega_2}{\omega_1 + \omega_2} \quad (4-1)$$

$$\beta = \xi \frac{2}{\omega_1 + \omega_2} \quad (4-2)$$

However, the achieved damping ratio based on Eq. (3) varies with the response frequency. To avoid overdamping the system response for the important modes of the system, in practical applications, the specified ω_1 and ω_2 are usually the minimum and maximum frequencies present in the system response (Chopra 2005). In this study, because the fundamental frequency of the system may vary during excitation, ω_1 and ω_2 are the system frequencies at the significant rocking and at the initial shaking stages, respectively. The specified ω_1 and ω_2 are determined by performing a dynamic analysis without considering any damping, followed by a short-time transfer function analysis to trace the variation of the system frequency with time. The short-time transfer function method is to divide the whole signals of input and output motions into many shorter time windows in equal length and then the transfer function for each time window can be built in terms of the Fourier's amplitude ratios of output/input motions

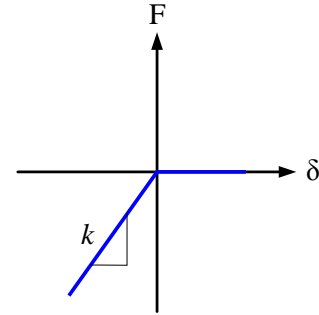


Fig. 5 Force-displacement relationship of gap element

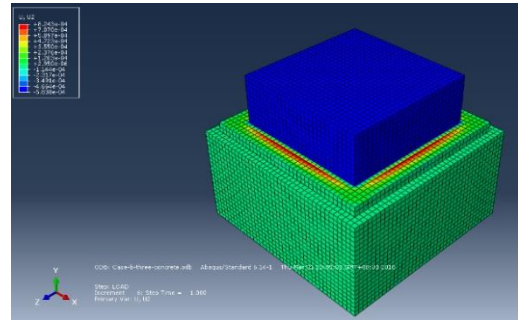


Fig. 6 ABAQUS modeling for determining k_v value of neoprene pad (CD40FS-R)

(amplification factors). The frequency corresponding to the peak value of the amplification factor defines the fundamental frequency of the system. Accordingly, the evolution of the fundamental frequency is built.

Dashpot damping model (for pier and foundation springs)

In contrast to the Rayleigh damping model, the dashpot damping model has more adaptability to set damping for the pier and foundation springs separately.

For the pier, a rotational dashpot is attached in parallel with each beam-column element for the elastic flexural response of the pier. Note that, for the plastic hysteretic response, the Takeda model is adopted, as described previously. The damping coefficient for the rotational dashpot is defined as

$$c = \frac{2\xi K}{\omega} \quad (5)$$

where ξ is the damping ratio, ω is the system frequency, and K is the rotational stiffness of the beam-column elements. Here, K is equal to EI/l , where EI is the flexural rigidity of the pier section and l is the beam-column element length.

For the foundation springs, Eq. (5) can also be applied to determine the damping coefficient by substituting the foundation spring stiffness (rotational spring stiffness for Models I and II or distributed spring stiffness for Models III and IV) for K .

As in the method adopted for the Rayleigh damping model, the system frequency ω in Eq. (5) is determined based on the range of the system frequencies obtained from a short-time transfer function analysis.

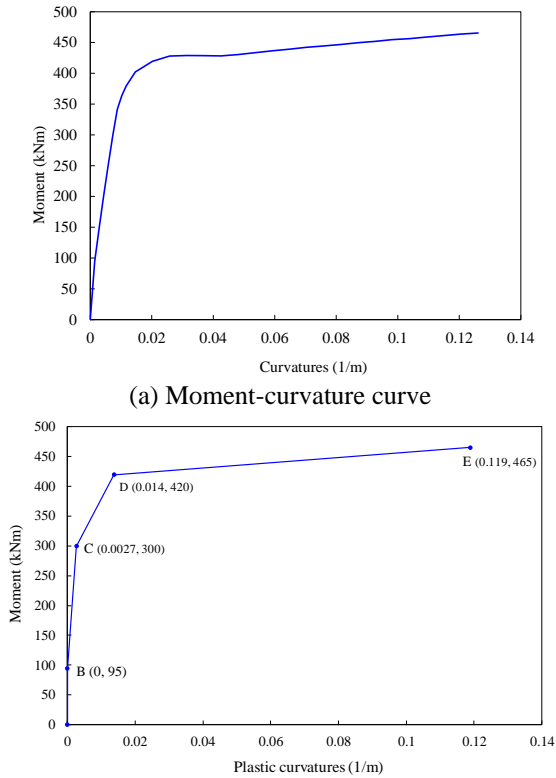


Fig. 7 Flexural property of pier section

4. Simulation results

Using the four numerical models outlined in the previous section, dynamic analyses are carried out on the dynamic responses of specimens CD40FS-R and CD40FB-R. A lumped mass of 55 t (equivalent weight of 539 kN) is attached on the top of the pier to represent the superstructure. Fifty beam-column elements with lengths of 0.05 m are adopted to simulate the pier. Based on the nonlinear stress-strain relationship of the reinforcing bars and concrete of the pier section, the moment-curvature curve of the pier section is calculated as displayed in Fig. 7(a). This moment-curvature curve is further simplified by a multi-linearized curve as shown in Fig. 7(b). Accordingly, a Young's modulus of 20.9 GPa is set and the plastic behavior of the pier is simulated using the distributed plastic hinge model with the hinge property shown in Fig. 7(b). Along the beam-column elements, fifty-one plastic hinges are set at the ends of the elements with plastic hinge lengths of 0.025 m for the elements at the pier ends and 0.05 m for the elements within the pier. Before dynamic analysis, pushover analyses are conducted to evaluate the appropriateness of the vertical subgrade reaction coefficient k_v by comparing the capacity curves of the pier with those from the cyclic pushover results. According to the k_v values from the previous ABAQUS analyses, the moment-rotation relationship for the rotational springs in CD40FS-R and CD40FB-R are determined as shown in Fig. 8. From the figure, for CD40FS-R, the moment and rotation corresponding initial uplift are around 134 kN-m and 0.00086 rad, respectively,

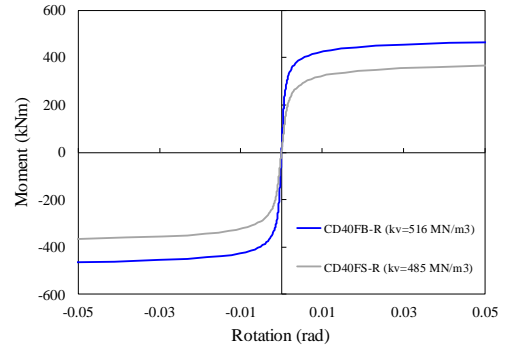


Fig. 8 Moment-rotation curves of rotational springs

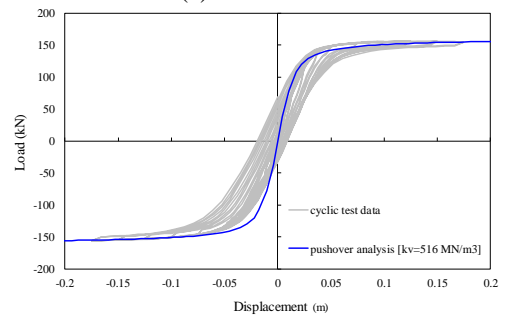
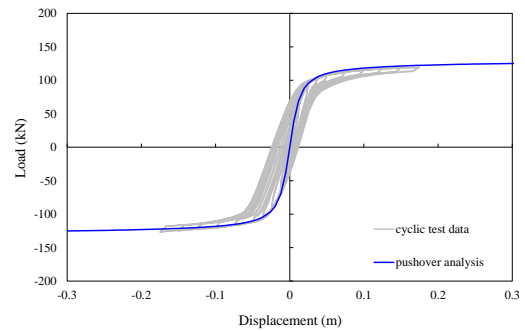


Fig. 9 Pushover results

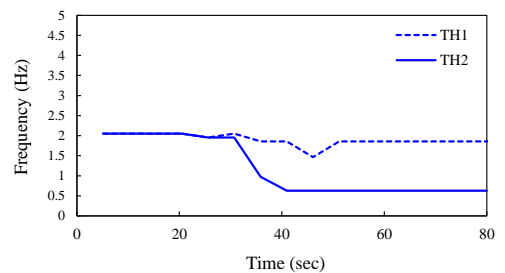
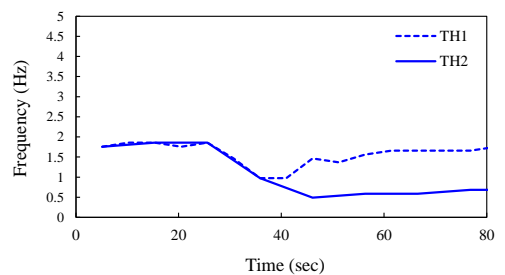
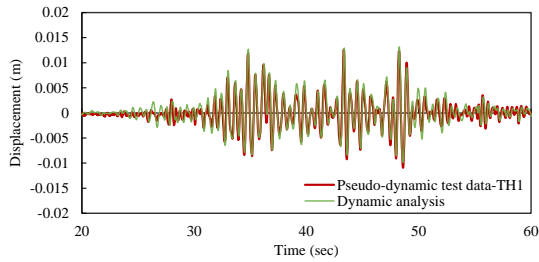
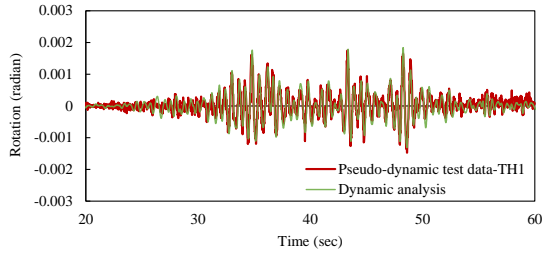


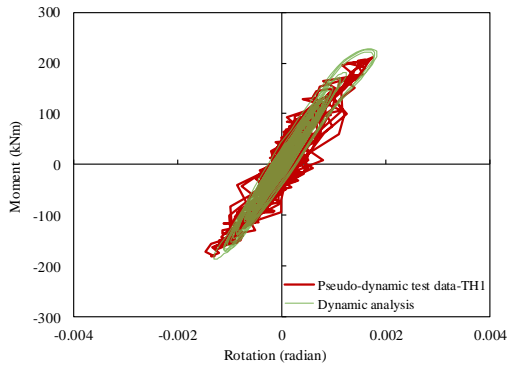
Fig. 10 Frequency-time plots



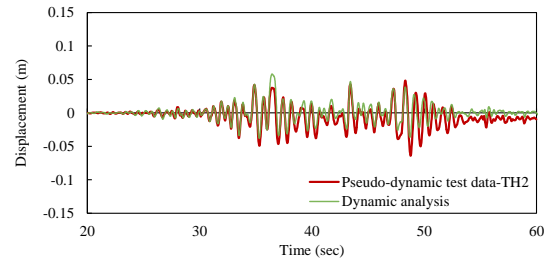
(a) Displacement history at the lumped mass



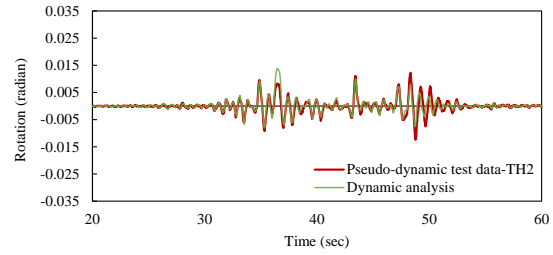
(b) Footing rotation history



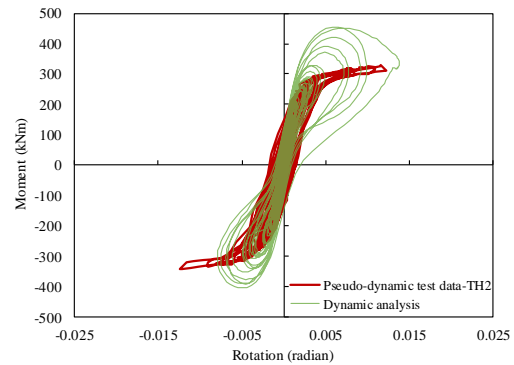
(c) Footing moment-rotation loops



(a) Displacement history at the lumped mass



(b) Footing rotation history



(c) Footing moment-rotation loops

Fig. 11 Dynamic analysis vs. test (CD40FS-R, Model I, TH1) Fig. 12 Dynamic analysis vs. test (CD40FS-R, Model I, TH2)

while for CD40FB-R, the moment and rotation corresponding initial uplift are around 166 kN-m and 0.00046 rad, respectively. As shown in Fig. 9, the numerical capacity curves for the small-size and large-size footings (CD40FS-R and CD40FB-R) are close to the backbone curve of the experimental curves.

For setting the damping model, Figs. 10(a) and (b) show the variation of the system frequency with time deduced according to the aforementioned analysis method. From the figure, ω_1 and ω_2 are set to be the lowest and highest frequencies, respectively, to represent the system frequencies at the significant rocking and at the initial shaking stages.

Next, the dynamic analysis results of the four models for specimens CD40FS-R and CD40FB-R are described and discussed in the following subsections.

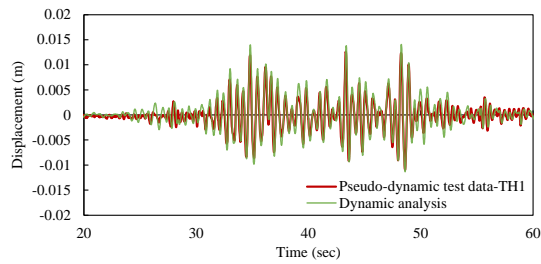
4.1 Specimen CD40FS-R

4.1.1 Model I

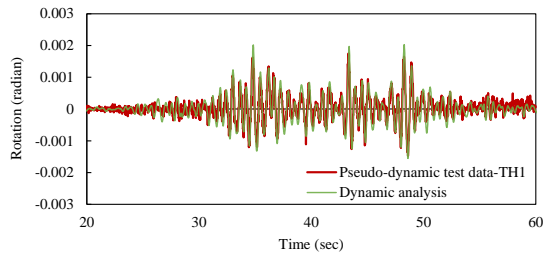
This model is the simplest and most commonly used model in practice. A rotational spring is used to simulate the foundation behavior and Rayleigh damping is applied to the whole system. According to Fig. 10(a), ω_1 and ω_2 for the TH1 input motion are respectively 6.136 and 11.655 rad/s

(0.977 and 1.855 Hz) and those for the TH2 input motion are respectively 4.295 and 11.655 rad/s (0.684 and 1.855 Hz). The damping ratio is determined to be 9% through calibration analyses with the pseudo-dynamic test results under the TH1 input motion (low intensity shaking). An initial value of 5% damping ratio is set, and then the damping ratio is updated until the analysis acceleration response matches the recorded.

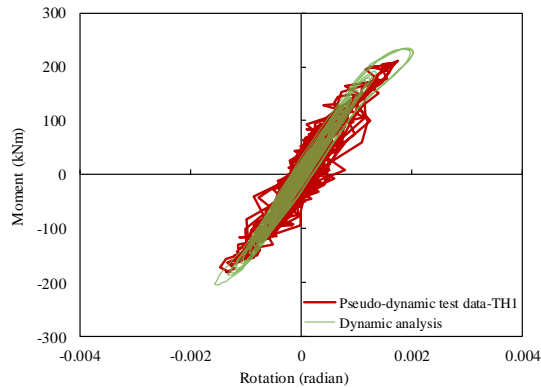
Based on these settings, the dynamic analysis is carried out to deduce the dynamic responses of the pier and footing. Fig. 11 displays the results for the TH1 input motion. Compared to the pseudo-dynamic test results, it is seen that the numerical results are close to the experimental ones in terms of the displacement of the lumped mass, the footing rotation and the hysteretic moment-rotation loops of the footing. Fig. 12 displays the results for the TH2 input motion. Compared to the pseudo-dynamic test results, it is seen that the numerical and experimental responses are close in terms of the displacement of the lumped mass and the footing rotation, except that the lumped mass in the experiment exhibits a slightly larger residual displacement at the end of the test. This residual displacement observed might be due to the slightly sliding of the specimen during the test. However, it is interesting to note that the moment-rotation curves have a significant deviation when the



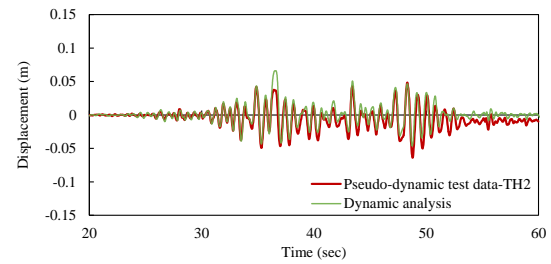
(a) Displacement history at the lumped mass



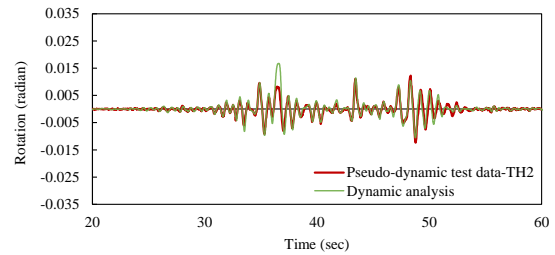
(b) Footing rotation history



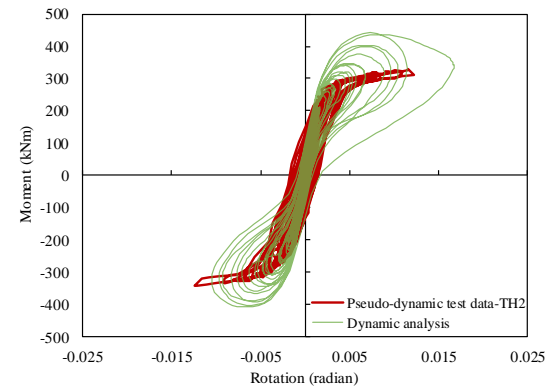
(c) Footing moment-rotation loops



(a) Displacement history at the lumped mass



(b) Footing rotation history



(c) Footing moment-rotation loops

Fig. 13 Dynamic analysis vs. test (CD40FS-R, Model II, TH1) Fig. 14 Dynamic analysis vs. test (CD40FS-R, Model II, TH2)

footing uplifts. The experimental results show that when the footing uplifts, the shape of the hysteretic loops becomes flat (with generally less energy dissipation), but the analysis result shows considerably large hysteretic loops. The maximum moment is overestimated by 32% and the energy dissipation (the area of the maximum hysteretic loop) is overestimated by 161%. The above difference is mainly attributed to that the energy dissipation mechanism of the rotational spring with viscous damping cannot properly represent the actual energy dissipation mechanism due to uplift. This simplified equivalent rotational spring model, in essence producing an elliptic hysteretic loop, cannot simulate the unique hysteretic shape due to the footing uplift although Rayleigh damping can reflect the change in rotational stiffness due to the uplift.

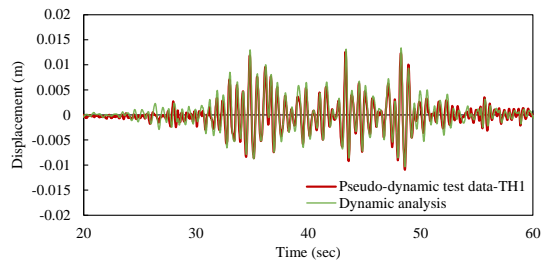
4.1.2 Model II

In Model II, the dashpot damping model is used to replace the Rayleigh damping model in Model I. To determine the damping coefficient in the dashpot model, $\omega = (\omega_1 + \omega_2)/2$ is applied. Through calibration with the results for the TH1 input motion, the damping ratios are found to be 5% and 4% for the pier and foundation spring, respectively.

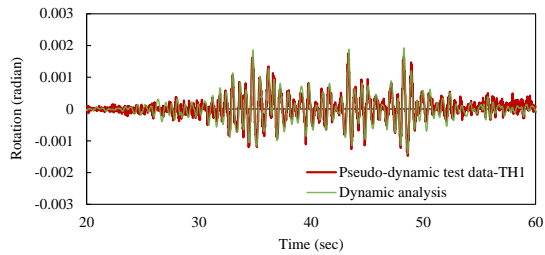
The results for Model II under the TH1 and TH2 input motions are shown in Figs. 13 and 14, respectively. It is seen that the numerical results and the measured lumped mass displacement and footing rotation are in good agreement. However, as shown in Fig. 14(c), for the TH2 input motion, the irrationally large energy dissipation at the two ends of the moment-rotation curve, as found in Model I, still occurs. The maximum moment is overestimated by 28% and energy dissipation is overestimated by 108%. Similar to Model I, this is because the dissipation mechanism of the equivalent rotational spring model cannot properly reflect the actual energy dissipation mechanism due to uplift.

4.1.3 Model III

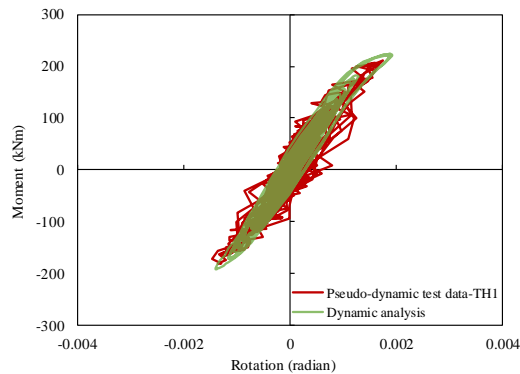
In place of the rotational spring model, Model III uses the distributed spring model to simulate the footing base reactions. The spring is composed of two elements linked in series: a gap element with a very large stiffness and a general two-way spring element. The stiffness of the two-way spring element is set to be k , multiplied by the tributary area of the spring. The Rayleigh damping model is used for the viscous damping of the whole system. The damping settings are the same as in Model I.



(a) Displacement history at the lumped mass

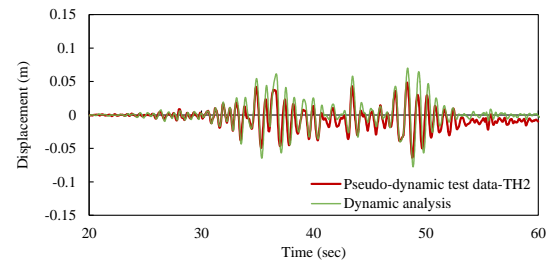


(b) Footing rotation history

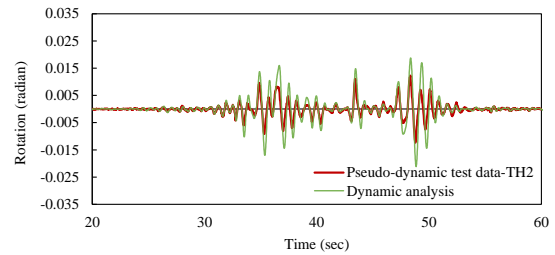


(c) Footing moment-rotation loops

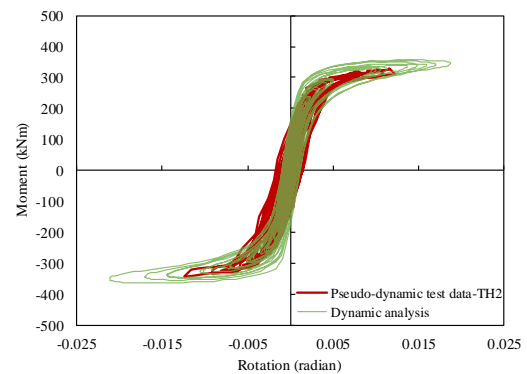
Fig. 15 Dynamic analysis vs. test (CD40FS-R, Model III, TH1)



(a) Displacement history at the lumped mass



(b) Footing rotation history



(c) Footing moment-rotation loops

Fig. 16 Dynamic analysis vs. test (CD40FS-R, Model III, TH2)

The results for Model III under the TH1 and TH2 input motions are shown in Figs. 15 and 16, respectively. The numerical and experimental results for the displacement of the lumped mass and the rotation of the footing show similar trends, except that a slightly larger footing rotation and pier displacement can be observed for the dynamic analysis when the footing uplifts significantly under the TH2 motion. Furthermore, as shown in Fig. 16(c), for the TH2 input motion, the pattern of the numerical hysteretic moment-rotation loops of the footing is similar to those of the experimental one. The maximum moment is overestimated by about 6% and the energy dissipation is overestimated by 69%. The irrational energy dissipation pattern from Models I and II is no longer observed, although slightly larger hysteretic loops occur when the footing uplifts.

4.1.4 Model IV

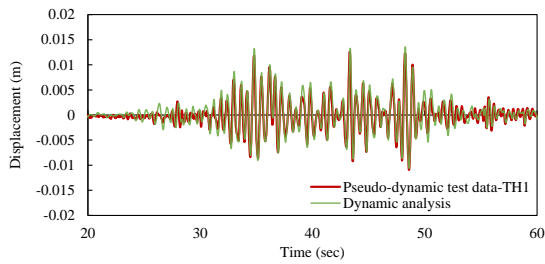
In Model IV, the distributed spring model is adopted for the foundation model as in Model III while the dashpot damping model is used in place of the Rayleigh damping model. In the distributed spring model, considering that the energy dissipation only occurs when the spring is in compression, each spring is composed of two elements

linked in series: a gap element with a very large stiffness and a general two-way spring-dashpot element. The stiffness of the two-way spring-dashpot element is set to be k_v , multiplied by the tributary area of the spring. The damping coefficients for the pier and foundation springs are computed based on Eq. (5) using $\omega = \omega_2$ (letting the distributed springs that are in compression provide sufficient damping when the footing significantly uplifts) and the same damping ratios as those adopted in Model II.

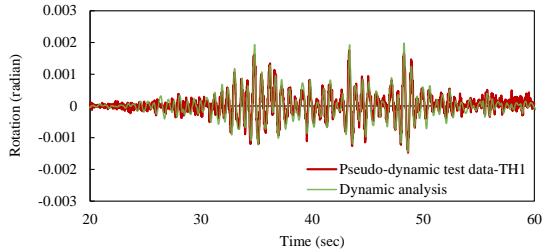
The results for Model IV under the TH1 and TH2 input motions are shown in Figs. 17 and 18, respectively. Compared to the results for Model III, the agreement between the numerical and experimental results is better, especially for the hysteretic moment-rotation loops. The maximum moment is overestimated by about 1% and the energy dissipation is overestimated by 34%. However, the footing rotation and pier displacement are still overestimated when a significant uplift of the footing occurs under the TH2 motion.

4.2 Specimen CD40FB-R

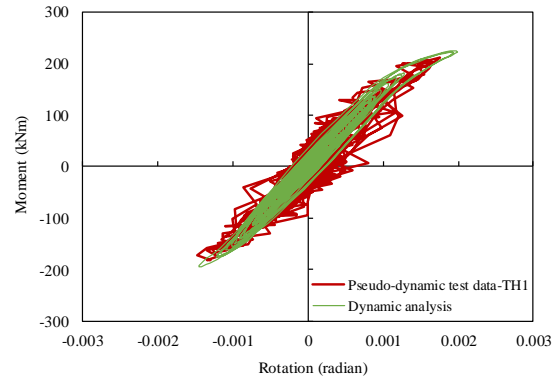
According to Fig. 10(b), ω_1 and ω_2 for the TH1 input motion are respectively 9.204 and 12.885 rad/s (1.465 and



(a) Displacement history at the lumped mass

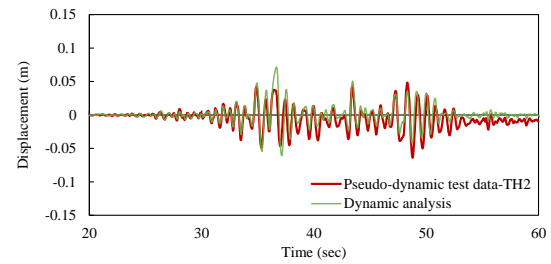


(b) Footing rotation history

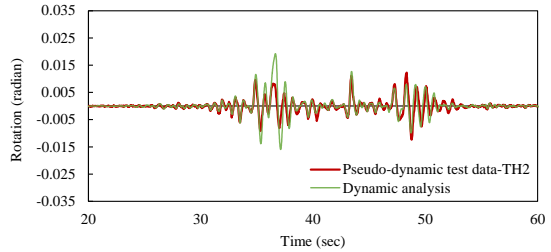


(c) Footing moment-rotation loops

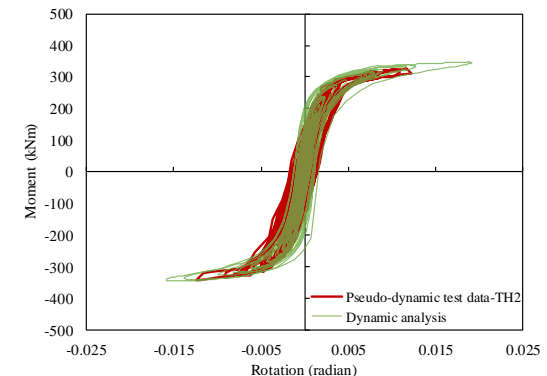
Fig. 17 Dynamic analysis vs. test (CD40FS-R, Model IV, TH1)



(a) Displacement history at the lumped mass



(b) Footing rotation history



(c) Footing moment-rotation loops

Fig. 18 Dynamic analysis vs. test (CD40FS-R, Model IV, TH2)

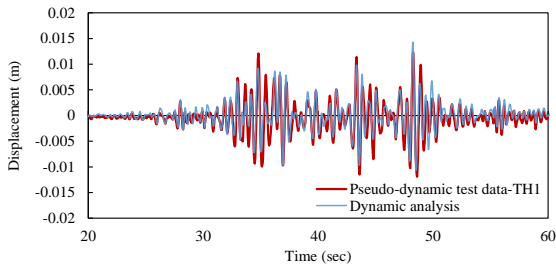
2.051Hz) and those for the TH2 input motion are respectively 3.94 and 12.885 rad/s (0.627 and 2.051Hz). The damping ratio is determined through calibration analyses with the TH1 pseudo-dynamic test results. The observations for the four models are similar to those for specimen CD40FS-R and thus, for brevity, they are not all discussed here. Figs. 19 and 20 display the results for Model IV under the TH1 and TH2 input motions. Generally, the numerical results are close to the experimental ones. In particular, the analysis results by Model IV can accurately capture the trend of the footing moment-rotation loops. Even though a slight overestimation in the slope of the moment-rotation loops under the TH1 input motion (may be due to an overestimation in the k_v) and an overestimation of the footing rotation and pier displacement (may be due to insufficient damping) are observed when the footing uplifts significantly under the TH2 input motion, this discrepancy can be improved by adjusting the value of k_v and damping ratio.

4.3 Discussions

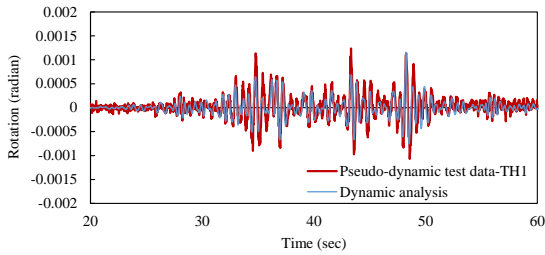
It is simpler to use an equivalent nonlinear rotational spring to represent the overall rocking behavior of a footing.

For the small excitation (TH1), the model can suitably simulate the seismic responses of the pier and its footing. However, although the nonlinear curve of the spring adopted reflects the uplift of the footing, the damping model cannot discern the differences in the energy dissipation mechanisms for the states before and after the footing uplifts. Therefore, as seen in the numerical results for Models I and II, the hysteretic moment-rotation loop of the footing cannot be suitably simulated regardless of the viscous damping model is used.

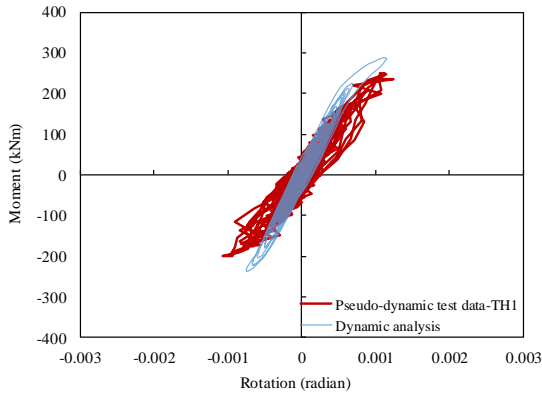
When the distributed spring model is used, the variation of the contact between the footing and the pad can be reflected in detail. The irrational dissipation during the uplift of the footing can be greatly improved. Before the uplift, the springs are linear and all the springs are in compression and contribute energy dissipation. Basically, the effects of the rotational spring model and distributed spring model are the same because of linear problems. Once the uplift occurs, the springs are still linear, but only the springs in compression contribute energy dissipation, and thus the moment-rotation response shows smaller hysteretic loops. Although the damping settings are the same for the rotational and distributed spring models, their effects are different even though the rotational spring uses a nonlinear



(a) Displacement history at the lumped mass

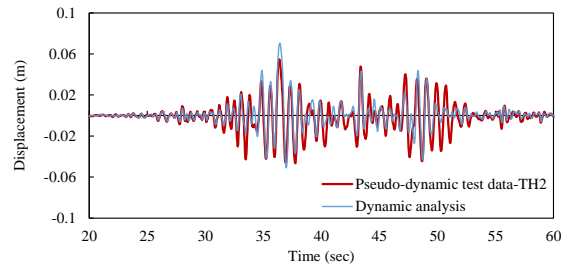


(b) Footing rotation history

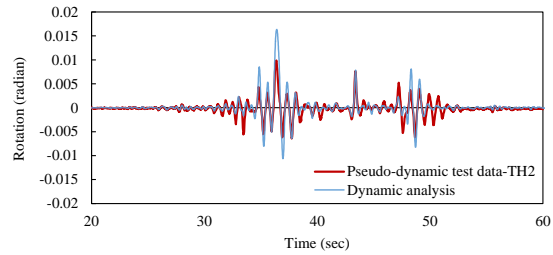


(c) Footing moment-rotation loops

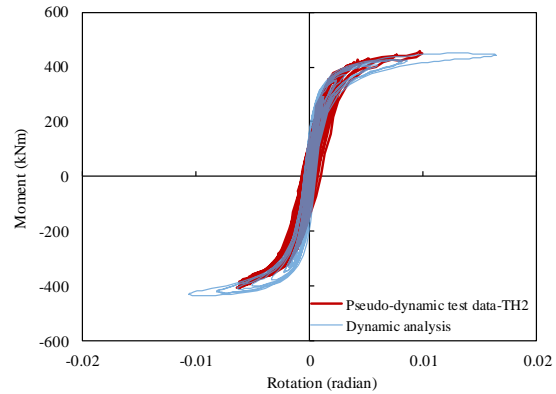
Fig. 19 Dynamic analysis vs. test (CD40FB-R, Model IV, TH1)



(a) Displacement history at the lumped mass



(b) Footing rotation history



(c) Footing moment-rotation loops

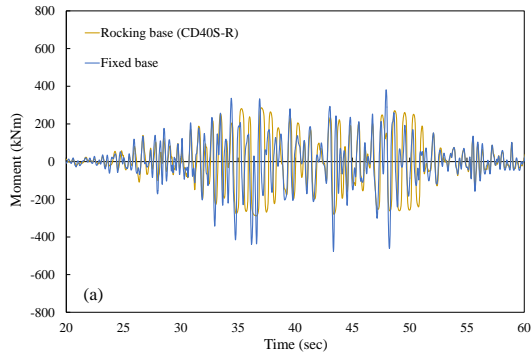
Fig. 20 Dynamic analysis vs. test (CD40FB-R, Model IV, TH2)

curve to represent the stiffness change during the uplift. Compared to the dashpot damping model whose damping is stiffness proportional, the Rayleigh damping model gives a larger energy dissipation because, in addition to the stiffness-proportional damping, the mass-proportional damping (the damping ratio is inversely proportional to the system frequency) also provides energy dissipation, especially when the footing significantly uplifts. For the dashpot damping model, since the damping ratio is linearly proportional to the system frequency, it contributes a smaller energy dissipation when the footing significantly uplifts and thus, the simulation of the moment-rotation hysteretic loops is better. Furthermore, the dashpot damping model has more adaptability than the Rayleigh damping model, as it can set respective damping coefficients for the pier and the foundation springs.

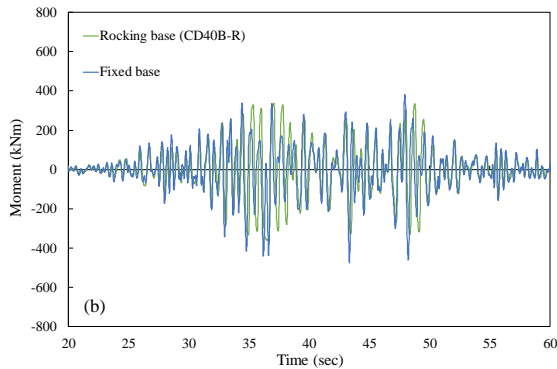
Overall, for the TH1 input motion, all the models (Models I-IV) can give rational predictions for the experimental results. For the TH2 input motion, because the footing significantly uplifts, the rotational spring model cannot suitably reflect the energy dissipation mechanism for the uplift of the footing, causing irrationally large energy dissipation at this stage.

5. Moment and damage responses of specimens

This section further investigates the detailed moment and damage responses of specimens CD40FS-R and CD40FB-R under the TH2 input motion. As observed in Fig. 8, the footing of specimen CD40-FS-R has a smaller moment capacity because of its smaller footing size. Therefore, the maximum moment at the pier base for CD40FS-R is less than that for CD40-FB-R, as displayed in Fig. 21, showing a more significant rocking effect and reducing the moment in the pier (the maximum moments are approximately 288 and 360 kNm for CD40FS-R and CD40FB-R, respectively). It is found that, when the footing is not allowed to rock, the fixed base condition will lead to a much larger moment (the maximum moment reaches approximately 477 kNm) than in the rocking base condition. Fig. 22 shows the development of plastic hinges for CD40FS-R and CD40FB-R at the end of shaking; different colors on the hinges show the degree of damage and the letters B and D represent the states of concrete cracking and reinforcement yielding of the pier section, respectively (refer to Fig. 7(b)). It is seen that CD40FS-R exhibits less damage and has a smaller residual



(a) CD40FS-R



(b) CD40FB-R

Fig. 21 Moment histories at pier bottom under rocking/fixed base conditions under TH2 motion

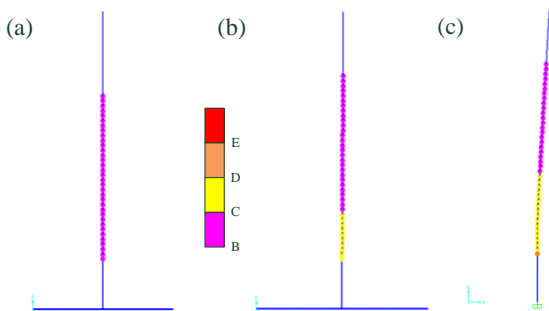
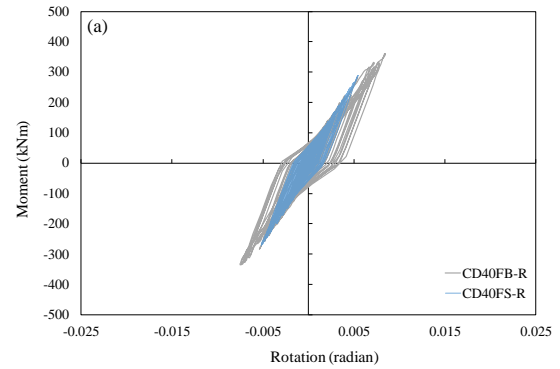
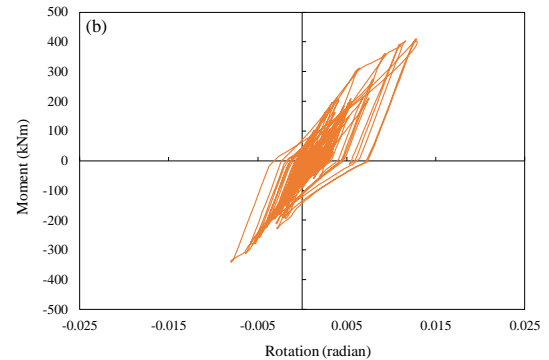


Fig. 22 Development of plastic hinges in the piers at the end of TH2 motion: (a) CD40FS-R, (b) CD40FB-R, (c) fixed base condition

displacement (only cracking occurs) than CD40FB-R because of the smaller moments induced in the pier. Fig. 22 also shows the development of the plastic hinges of the pier in the fixed base condition, showing that the pier is severely damaged (that is, yielding occurs) and has a remarkable residual displacement. The comparison of the ranges of the plastic hinges between the rocking and fixed base conditions implies that a rocking base can help protect the pier from excessive damage. However, it should be noted that CD40FS-R has a larger displacement at the top of the pier than CD40FB-R does as shown in Figs. 18(a) and 19(b). Fig. 23(a) shows the hysteretic moment-rotation loops of the plastic zone near the pier bottoms of CD40FS-R and CD40FB-R. It can be seen that the piers also contribute to energy dissipation due to cracking, in that the loops of CD40FB-R are larger because of the greater degree



(a) CD40-FS-R and CD40-FB-R



(b) Fixed base condition

Fig. 23 Hysteretic moment-rotation loops of plastic zone

of cracking developed in the pier. Furthermore, when the pier is in the fixed base condition, it exhibits more significant hysteretic loops, as shown in Fig. 23(b), because all the earthquake energy is sustained by the pier, which causes the pier to be more severely damaged.

6. Conclusions

In this study, numerical analyses were performed to simulate pseudo-dynamic tests on two rocking-base bridge piers with different footing sizes. Four types of numerical models were established, considering the nonlinear behavior of the pier and different types of foundation modeling and viscous damping models. From this study, it is found that, when the footing does not uplift, all the four models yield accurate predictions, but once the footing uplifts, Models I and II, which use the equivalent rotational spring model, fail to provide a rational energy dissipation mechanism. The rotational spring model is generally suitable in static pushover analysis to determine the capacity curves of a pier; however, it does not suitably capture the hysteretic moment-rotation response of the footing in the dynamic analyses. Although the rotational spring model can reflect the effect of footing uplift using a nonlinear moment-rotation curve, as used in static pushover analysis, it cannot consider different energy dissipation mechanisms for the states before or after the uplift of the footing. On the other hand, although the distributed spring model is more complicated, it can provide a more rational energy dissipation behavior during the footing uplift. The

dashpot damping model allows energy dissipation to occur only in the springs that are in compression and it has more flexibility in setting the damping for the pier and the foundation springs.

Therefore, to appropriately simulate the foundation rocking behavior for a footing on a firm ground condition, the distributed spring model with the dashpot damping model for the foundation soil is recommended. Since the damping coefficient in the dashpot damping model is dependent on the system frequency, a dynamic analysis without considering any damping together with a short-time transfer function analysis can be performed to trace the variation of the system frequency with time.

From the analyzed moment and damage responses of the piers subjected to strong seismic loading, it is found that the anticipated foundation rocking is helpful in reducing the moment demand of the piers and that it can protect the piers from excessive damage, but its effect will decrease with increasing footing size. Therefore, the pier on a larger footing sustains a larger moment demand. Since the cracking moment of the pier section is much lower than the moment capacity of the footing, the piers are susceptible to cracking damage and the induced plastic response can also provide some contribution to earthquake energy dissipation.

Acknowledgments

The authors would like to thank the Ministry of Science and Technology of Taiwan (Grant no. MOST 104-2221-E-002-218) and the National Taiwan University (Grant no. NTUCC-107L892507) for financial support.

References

- Allotey, N. and El Naggar M.H. (2003), "Analytical moment-rotation curves for rigid foundations based on a Winkler model", *Soil Dyn. Earthq. Eng.*, **23**, 367-381. [https://doi.org/10.1016/S0267-7261\(03\)00034-4](https://doi.org/10.1016/S0267-7261(03)00034-4).
- Allotey, N. and El Naggar, M.H. (2007), "An investigation into the Winkler modeling of the cyclic response of rigid footings", *Soil Dyn. Earthq. Eng.*, **28**, 44-57. <https://doi.org/10.1016/j.soildyn.2007.04.003>.
- American Society of Civil Engineers (ASCE) (2000), FEMA-356-Prestandard and Commentary for the Seismic Rehabilitation of Buildings, Washington, DC.
- Anastasopoulos, I. and Kontoroupi, Th. (2014), "Simplified approximated method for analysis of rocking systems accounting for soil inelasticity and foundation uplifting", *Soil Dyn. Earthq. Eng.*, **56**, 28-43. <https://doi.org/10.1016/j.soildyn.2013.10.001>.
- Antonellis, G., Gavras, A.G., Panagiotou, M., Kutter, B.L., Guerrini, G., Sander, A.C. and Fox, P.J. (2015), "Shake table test of large-scale bridge columns supported on rocking shallow foundations", *J. Geotech. Geoenviron. Eng.*, **141**(5), 04015009. [https://doi.org/10.1061/\(ASCE\)GT.1943-5606.0001284](https://doi.org/10.1061/(ASCE)GT.1943-5606.0001284).
- Apostolou, M., Gazetas, G. and Garini, E. (2007), "Seismic response of slender rigid structures with foundation uplift", *Soil Dyn. Earthq. Eng.*, **27**(7), 642-654. <https://doi.org/10.1016/j.soildyn.2006.12.002>.
- Billington, S.L. and Yoon, J.K. (2004), "Cyclic response of unbonded posttensioned precast columns with ductile fiber-reinforced concrete", *J. Bridge Eng.*, **9**(4), 353-363. [https://doi.org/10.1061/\(ASCE\)1084-0702\(2004\)9:4\(353\)](https://doi.org/10.1061/(ASCE)1084-0702(2004)9:4(353)).
- Chaudhary, M.T.A. (2017), "Seismic response of bridges supported on shallow rock foundations considering SSI and pier column inelasticity", *KSCE J. Civil Eng.*, **21**(1), 285-295. <https://doi.org/10.1007/s12205-016-0352-5>.
- Chen, S.J., Yang, K.C., Lin, K.M. and Wang, C.D. (2011), "Seismic behavior of ductile rectangular composite bridge piers", *Earthq. Eng. Struct. Dyn.*, **40**, 21-34. <https://doi.org/10.1002/eqe.1018>.
- Chiou, J.S., Chen, C.H. and Hwang, Y.W. (2018), "Pushover and shaking table tests on a rocking-governed column-footing model on dry dense sand", *J. Chin. Inst. Eng.*, **41**(3), 247-258. <https://doi.org/10.1080/02533839.2018.1454858>.
- Chiou, J.S., Yang, H.H. and Chen, C.H. (2009), "Use of plastic hinge model in nonlinear pushover analysis of a pile", *J. Geotech. Geoenviron. Eng.*, **135**(9), 1341-1346. [https://doi.org/10.1061/\(ASCE\)GT.1943-5606.0000015](https://doi.org/10.1061/(ASCE)GT.1943-5606.0000015).
- Chopra, A.K. (1995), *Dynamics of Structures*, Upper Saddle River, Prentice-Hall, NJ.
- Computer & Structures Inc. (2017), SAP2000, Integrated Software for Structural Analysis and Design [computer program], Computer & Structures, Inc., Berkeley, Calif.
- Deng, L., Kutter, B.L. and Kunnath, S.K. (2012), "Probabilistic seismic performance of rocking-foundation and hinging-column bridges", *Earthq. Spectra*, **28**(4), 1423-1446. <https://doi.org/10.1193/1.4000093>.
- Deng, L., Kutter, B.L. and Kunnath, S.K. (2014), "Seismic design of rocking shallow foundations: displacement-based methodology", *J. Geotech. Geoenviron. Eng.*, **19**(11), 04014043-1-11. [https://doi.org/10.1061/\(ASCE\)BE.1943-5592.0000616](https://doi.org/10.1061/(ASCE)BE.1943-5592.0000616).
- Gajan, S. and Kutter, B.L. (2008), "Capacity, settlement, and energy dissipation of shallow footings subjected to rocking", *J. Geotech. Geoenviron. Eng.*, **134**(8), 1129-1141. [https://doi.org/10.1061/\(ASCE\)1090-0241\(2008\)134:8\(1129\)](https://doi.org/10.1061/(ASCE)1090-0241(2008)134:8(1129)).
- Galal, K. (2007), "Lateral force-displacement ductility relationship of non-ductile squat RC columns rehabilitated using FRP confinement", *Struct. Eng. Mech.*, **25**(1), 75-89. <https://doi.org/10.12989/sem.2007.25.1.075>.
- Grange, S., Kotronis, P. and Mazars J. (2008), "A macro-element for a shallow foundation to simulate soil-structure interaction considering uplift", *Comptes Rendus Mecanique*, **336**, 856-862. <https://doi.org/10.1016/j.crme.2008.10.002>.
- Hibbit, Karlsson & Sornsen Inc. (2000), ABAQUS Theory and User's Manual-Version 6.1, Hibbit, Karlsson & Sornsen, Pawtucket, R.I.
- Hung, H.H., Liu, K.Y., Ho, T.H. and Chang, K.C. (2011), "An experimental study on the rocking response of bridge piers with spread footing foundations", *Earthq. Eng. Struct. Dyn.*, **40**(7), 749-769. <https://doi.org/10.1002/eqe.1057>.
- Hung, H.H., Liu, K.Y., Ho, T.H. and Chang, K.C. (2014), "Rocking behavior of bridge piers with spread footings under cyclic loading and earthquake excitation", *Earthq. Struct.*, **7**(6), 1001-1024. <https://doi.org/10.12989/eas.2014.7.6.1001>.
- Japan Road Association (JRA) (2012), Design Specifications for Highway Bridges - IV: Substructures. (in Japanese)
- Lu, Y., Marshall A.M. and Hajirasoulihaand I. (2016), "A simplified nonlinear sway-rocking model for evaluation of seismic response of structures on shallow foundations", *Soil Dyn. Earthq. Eng.*, **81**, 14-26. <https://doi.org/10.1016/j.soildyn.2015.11.002>.
- Luo, X., Murono, Y. and Nishimura, A. (2002), "Verifying adequacy of the seismic deformation method by using real examples of earthquake damage", *Soil Dyn. Earthq. Eng.*, **22**, 17-28. [https://doi.org/10.1016/S0267-7261\(01\)00053-7](https://doi.org/10.1016/S0267-7261(01)00053-7).
- Mergos, P.E. and Kawashima, K. (2005), "Rocking isolation of a

- typical bridge pier on spread foundation”, *J. Earthq. Eng.*, **9**(2), 395-414. <https://doi.org/10.1142/S1363246905002456>.
- Ni, P. (2013), “Effects of soil-structure interaction on direct displacement based assessment procedure of multi-span reinforced concrete bridges”, *Eur. J. Environ. Civ. Eng.*, **17**(7), 507-531. <https://doi.org/10.1080/19648189.2013.771111>.
- Raychowdhury, P. and Hutchinson, T.C. (2009), “Performance evaluation of a nonlinear Winkler-based shallow foundation model using centrifuge test results”, *Earthq. Eng. Struct. Dyn.*, **38**, 679-698. <https://doi.org/10.1002/eqe.902>.
- Sakellarakis, D. and Kawashima, K. (2006), “Effectiveness of seismic rocking isolation of bridges based on shake table test”, *First European Conf. on Earthquake Engineering and Seismology, European Association for Earthquake Engineering*, Istanbul, Turkey.
- Shirato, M., Kouno, T. and Asai, R., Nakatani, S., Fukui, J. and Paolucci, R. (2008), “Large-scale experiments on nonlinear behavior of shallow foundations subjected to strong earthquakes”, *Soil. Found.*, **48**(5), 673-692. <https://doi.org/10.3208/sandf.48.673>.
- Standards New Zealand (2004), Structural Design Actions, NZS 1170.5: 2004, Wellington, New Zealand.
- Takeda, T., Sozen, M.A. and Nielsen, N.N. (1970), “Reinforced concrete response to simulated earthquakes”, *J. Struct. Div.*, **96**(12), 2557-2573.
- Terzaghi, K. (1955), “Evaluation of coefficients of subgrade reaction”, *Geotechnique*, **5**(4), 297-326. <https://doi.org/10.1680/geot.1955.5.4.297>.
- Wang, Z., Ge, J. and Wei, H. (2014), “Seismic performance of precast hollow bridge piers with different construction details”, *Front. Struct. Civil Eng.*, **8**(4), 399-413. <https://doi.org/10.1007/s11709-014-0273-7>.